Electrodeposition of Fe and Composite Fe/ZrO_2 Coatings from a Methanesulfonate Bath

V. S. Protsenko[a], E. A. Vasil'eva[a], I. V. Smenova[a], A. S. Baskevich[a], I. A. Danilenko[b], T. E. Konstantinova[b], and F. I. Danilov[a]

[a] *Ukrainian State University of Chemical Technology, Gagarin, Av 8, Dnepropetrovsk, 49005, Ukraine, e-mail: Vprotsenko7@gmail.com*
[b] *Donetsk Institute for Physics and Engineering named after O.O. Galkin of the NAS of Ukraine, R. Luxembourg, str. 72, Donetsk, 83114, Ukraine*

The electrodeposition of iron and composite iron-zirconia coatings from a methanesulfonate electrolyte was investigated. The current efficiency of iron deposition reaction was stated to be sufficiently higher in methanesulfonate electrolytes than in usual sulfate baths. Iron coatings electrodeposited from a methanesulfonate bath have a nano-crystalline structure. The Fe coatings obtained from methanesulfonate baths are harder than those deposited from sulfate baths because of the strengthening effect by the Hall-Petch mechanism. The composite Fe/ZrO_2 coatings can be obtained from the iron electroplating baths containing the particles of zirconia stabilized by 3 mol % yttria. The kinetics of ZrO_2 particles co-deposition with iron in methanesulfonate electrolytes obeys Guglielmi's model. The insertion of zirconia particles into the iron matrix results in an appreciable increase of the coatings microhardness via the dispersion strengthening mechanism.

Keywords: electroplating, iron, zirconia, composite coating, methanesulfonate electrolyte.

УДК 544.65:621.357

INTRODUCTION

The electrodeposition of iron, its alloys and composites has been widely used for various engineering applications such as electrotypes, electroforming, repairing worn and corroded machine parts, magnetics components in computer and electronic industries, etc. [1–7]. Iron electrodeposits are usually obtained from acid sulfate, chloride, fluoroborate, and sulfamate Fe(II) electrolytes. Acid iron electroplating baths are well studied. They are highly productive and their compositions are relatively simple. Nevertheless, acid electrolytes for iron electrodeposition are rather corrosive and toxic; therefore, the development of novel acid Fe(II) baths is an important problem of modern electroplating.

Aqueous Fe(II) baths on the base of methanesulfonic acid CH_3SO_3H (MSA) seem to be an attractive and perspective alternative to common iron electroplating baths since MSA is considered to be a "green acid" due to its environmental advantages [8]. MSA is known to be far less corrosive and toxic than the usual mineral acids used in different branches of industry [9]. Methanesulfonates of various metals are highly soluble in water; the conductivity of the corresponding aqueous solutions is high. In addition, MSA is easily biodegradable. Because of these advantages, electrochemical systems on the base of MSA and its salts have been shown to be very promising for different electrochemical technologies, and especially for electroplating of some metals and alloys [10–15].

However, only several papers have been published, in which the electrodeposition of iron from methanesulfonate baths was investigated [16–18]. Thus, it has been revealed that methanesulfonate iron plating baths ensure a wide range of operating current densities and reduced hydrogen saturation of coatings [16]. The application of MSA-containing iron plating baths was shown to provide satisfactory adhesion of iron coatings with steel and cast iron [17]. Nevertheless, the data presented in those studies are very limited. The effects of deposition conditions on Fe electroplating from methanesulfonate electrolytes remain practically unexplored.

The performance characteristics of iron-based electrodeposits may be sufficiently improved by the incorporation of inert particles into metallic coatings (i.e. when depositing composite coatings) [6, 7, 19]. We report here the results of our attempts to prepare composite Fe/ZrO_2 coatings. Zirconia is of a persistent interest as an engineering material because of its outstanding combination of properties such as: strength, toughness, high melting point, chemical inertness, hardness, etc. The electrodeposition of zirconia-containing composite coatings with Ni and other matrices has been described in a number of papers [20–22]. Composite Ni/ZrO_2 coatings exhibit improved physicochemical and service properties compared with those of the pure nickel under the same electrodeposition conditions.

In our recent work [23], we have demonstrated that the ZrO_2-containing hard composite coatings on the base of the iron matrix may be electrodeposited

using methanesulfonate electrolytes. However, the kinetics of iron-based composite coatings from MSA-containing electrochemical systems and the hardening mechanism remain still undetermined. Thus, the purpose of this work is to study the kinetics and mechanism of Fe and composite Fe/ZrO_2 electrodeposition processes from MSA-containing plating baths. The effects of different factors on the microhardness of deposits obtained and probable hardening mechanisms are also revealed and discussed.

EXPERIMENTAL

All solutions were prepared using twice-distilled water and reagent grade chemicals. Iron (II) methanesulfonate was synthesized by the procedure described in detail in [8]. The pH value of the plating bath was controlled through a common potentiometric method. If needed, the pH of the bath was adjusted to the required value by adding either Na_2CO_3 or MSA solutions. The concentration of Fe(II) ions in the plating bath was determined by the titrometric analysis. To this end, $K_2Cr_2O_7$ solution was used as a titrant in the presence of difenilaminsulfonat as a redox indicator.

Electrodeposition was performed at a steady current density in a usual thermostated glass cell. Iron and iron-zirconia films were deposited both on the mild steel plates and on the disc electrode of the copper foil (S = 1 cm^2) fixed in a plastic holder. Prior to each experiment, the cathode surface was treated with magnesium oxide, etched for several minutes in 1:1 (vol.) hydrochloric acid solution and then thoroughly rinsed with twice-distilled water. The electrolysis was carried out with anodes made from mild steel. The current efficiency of iron deposition was calculated from the cathode gain in weight.

Voltammetric measurements were performed using Potentiostat/Galvanostat Reference 3000 (Gamry) in a conventional glass three-electrode cell deaerated by blowing with electrolytic hydrogen. The electrochemical cell was thermostated by a thermostat Flüssigkeitsthermostate Baureihe U/UH8. The cathode and anodic compartments were separated by a porous glass diaphragm. A freshly electrodeposited Fe layer with a thickness of 15 μm on the platinum substrate was used as the working electrode (S = 0.28 cm^2). The counter electrode was made of the platinum wire. All potentials were measured with respect to the saturated Ag/AgCl-electrode and recalculated to a standard hydrogen electrode.

For obtaining composite coatings, the doped zirconia nanopowder ZrO_2+3 mol% Y_2O_3 was incorporated into the electrodeposition bath. Zirconia nanopowder was synthesized via co-precipitation technique from $ZrOCl_2 \cdot nH_2O$ and $Y(NO_3)_3$ salts. The details of this procedure were published elsewhere [24–26]. The procedure allowed obtaining mono-dispersed nanopowders of stabilized zirconia with a prescribed particle size of about 18 nm. It should be noted that doping by 3 mol % Y_2O_3 is used in order to stabilize the tetragonal phase of zirconia [26].

The sedimentation analysis of the size of ZrO_2 particles in the suspensions was performed with a digital analytical balance Vibra HT-120 (Shinko denshi).

The surface morphology of deposits was investigated by the scanning electron microscopy (SEM) utilizing scanning electron microscope JSM-6490. In order to choose a typical picture for each coating, four to six locations (in the central zone) were taken.

The chemical composition of Fe/ZrO_2 composite layers was determined both by the energy dispersive X-ray (EDX) microanalyser coupled to the SEM instrument and by the chemical analysis. In the latter case, a coating obtained on the copper substrate was solved in sulfuric acid (1:1 vol.) and then the solution was titrated according to the procedure described above.

The X-ray diffraction (XRD) analysis was performed by an X-ray diffractometer DRON-3.0 in the monochromatized Cu-K_α radiation. The crystalline size was estimated by the Scherrer equation.

Vickers microhardness (HV) was determined using a PMT-3 apparatus at a 100 g load, the coating thickness being not less than 20 μm. The average value of the deposits microhardness was calculated from more than 10 separate measurements.

RESULTS AND DISCUSSION

Electrodeposition of iron from methanesulfonate electrolyte

Iron electrodeposition from methanesulfonate baths has not been sufficiently described in literature so far. Therefore, it is reasonable to characterize the main features of electroplating process in this system in comparison with a "common" sulfate bath.

The current efficiency (CE) increases with the current density both in a methanesulfonate electrolyte and in the sulfate one (Fig. 1). However, the growth of the CE values ceases in MSA-containing bath at i > 20 A/dm^2. We have stated that an increase in the bath temperature leads to a decrease in the CE values [23].

All other conditions being equal, the current efficiency in MSA-containing electrolyte is considerably higher than that in case of the sulfate bath. This is the most evident advantage of the methanesulfonate system over the sulfate one.

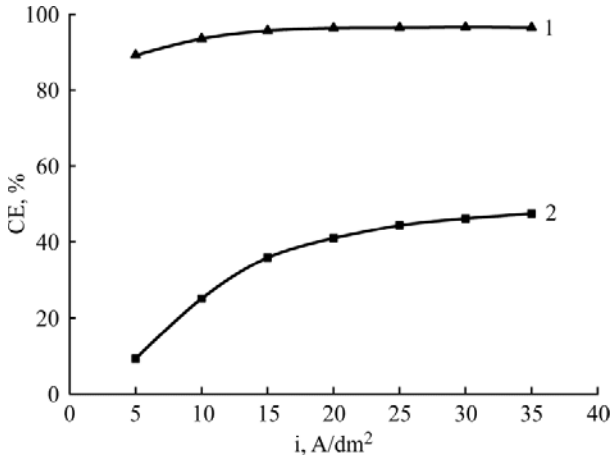

Fig. 1. Effect of current density on current efficiency of Fe electrodeposition from (1) methanesulfonate electrolyte containing 1.25M $Fe(CH_3SO_3)_2$ and (2) sulfate electrolyte containing 1.25M $FeSO_4$. Bath temperature 298K, pH 1.3.

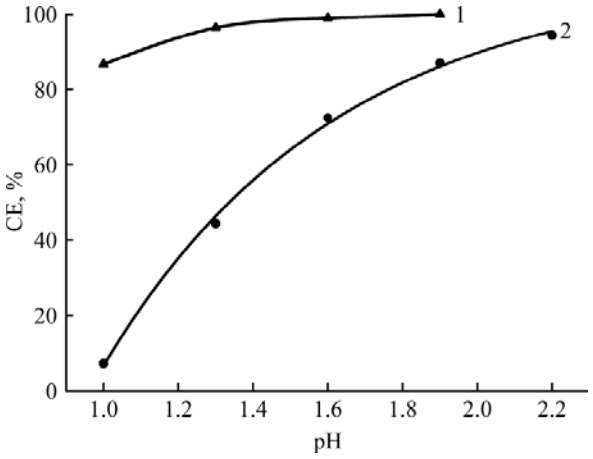

Fig. 2. Effect of pH on current efficiency of Fe electrodeposition from (1) methanesulfonate electrolyte containing 1.25M $Fe(CH_3SO_3)_2$ and (2) sulfate electrolyte containing 1.25M $FeSO_4$. Bath temperature 298K. Current density 25 A/dm^2.

The nature of anion affects the surface appearance of deposits. Dull coatings are obtained from sulfate electrolytes and bright iron coatings deposits from MSA-containing plating baths.

The CE of iron electrodeposition increases with an increase in the bath pH (Fig. 2), this dependence is more sharply pronounced for the sulfate electrolyte. At a high acidity (pH 1.0), the CE in the methanesulfonate system is about 90%, while it approaches only about 8% in the sulfate bath. It should be stressed that an increase in the electrolyte pH is not desirable in consideration of the increase of the rate of Fe(II) ions oxidation by atmospheric oxygen. At pH > 1.5, a rapid oxidation of Fe(II) is especially noticeable and iron deposits become dark and rough. Taking into account all these facts, one may assume that the bath pH should be equal to about 1.3.

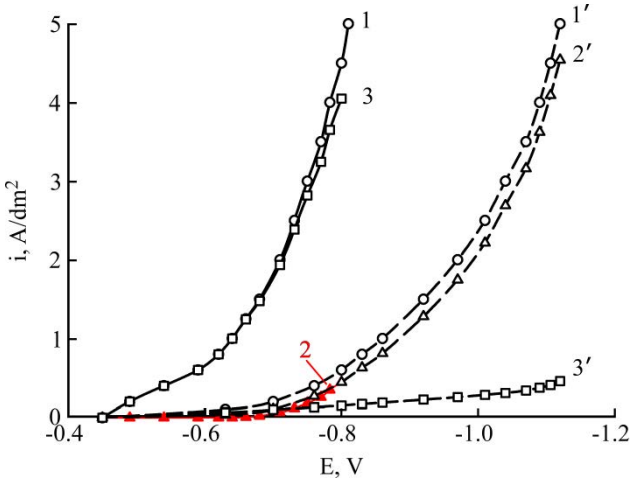

Fig. 3. Steady-state polarization curves obtained in (1)–(3) sulfate electrolyte containing 1.25M $FeSO_4$ and (1')–(3') methanesulfonate electrolyte containing 1.25M $Fe(CH_3SO_3)_2$. (1) and (1') – total current density; (2) and (2') – partial current density of iron deposition; (3) and (3') – partial current density of hydrogen evolution reaction. Bath temperature 298K, pH 1.3.

The iron deposition reaction in acid aqueous solutions is always accompanied by the hydrogen evolution reaction (HER):

$$Fe^{+2} + 2e^- \rightarrow Fe, \quad (1)$$

$$2H^+ + 2e^- \rightarrow H_2. \quad (2)$$

Hence, detected differences in the CE values of iron deposition for the two electroplating baths under consideration may be associated with some differences in the kinetics of the parallel electrochemical reactions (1) and (2). Figure 3 gives partial-polarization curves of iron electrodeposition and of the HER. As can be seen, the kinetics of Fe(II) ions discharge in the methanesulfonate and sulfate systems is similar since the respective partial-polarization curves almost coincide. Meanwhile, the hydrogen evolution reaction in MSA containing electrolyte occurs with a significantly higher cathode polarization than in the sulfate bath. This is due to some differences in the chemical properties of MSA and sulfuric acid. Indeed, MSA is a monobasic strong acid (pK_a = 21.9) [8] while, H_2SO_4 is a dibasic acid in whose aqueous solutions both sulfate and bisulfate anions are present. As shown in [27], the current density of the proton reduction in acid Fe(II) sulfate electrolytes was higher than that measured in chloride or perchlorate solutions at the same pH value. The difference was explained by the presence of bisulfate ions since the following chemical equilibrium exists in the sulfate electrolytes:

$$HSO_4^- \Leftrightarrow H^+ + SO_4^{2-} \quad pK = 1.99. \quad (3)$$

The bisulfate ion acts as a proton source. Thus, both "free" proton ions and those generated from the dissociation of HSO_4^- ions may take part in the hydrogen evolution reaction. The appearance of an additional proton source in a solution leads to an increase in the current density of the HER. Evidently, such phenomenon cannot occur in methanesulfonate electrolytes. A higher partial current density of the HER in sulfate baths is the reason of the low CE of the Fe deposition reaction when compared with the MSA-containing baths.

Sedimentation analysis of the size of dispersed phase particles

In accordance with [19], the composition and properties of composite electrodeposits are determined, to a large extent, by the dimensions of dispersed phase particles. As stated above, the monodispersed nanopowder of yttria-stabilized zirconia with a prescribed particle size of 18 nm was used to produce composite coatings. However, it is well known that the addition of electrolytes to a colloidal system leads to particle aggregation. The size of dispersed phase particles in iron plating baths was determined sedimentometrically. As follows from the data presented in Fig. 4, the colloidal systems both in a methanesulfonate electrolyte and in a sulfate one become polydispersed. The main fraction of the suspension contains particles with the aggregate size of about 3 μm.

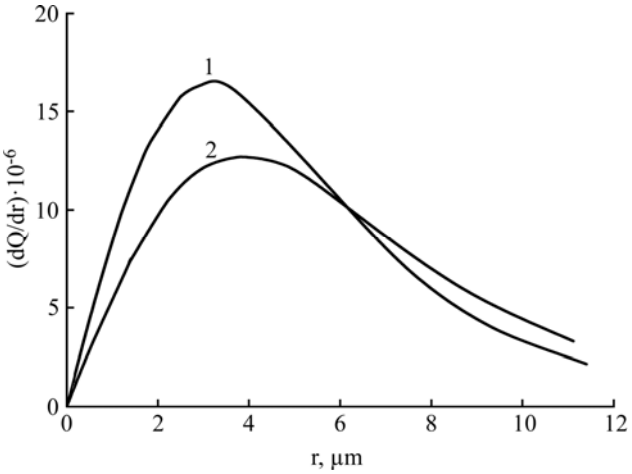

Fig. 4. Differential curves of particle size distribution: (1) in methanesulfonate electrolyte containing 1.25M $Fe(CH_3SO_3)_2$, 20 g/dm^3 ZrO_2; (2) in sulfate electrolyte containing 1.25M $FeSO_4$, 20 g/dm^3 ZrO_2. Bath temperature 298K, pH 1.3.

Such behavior may be explained by the DLVO (Derjaguin, Landau, Verwey, Overbeek) theory whereby the compression of the double layer, when increasing ionic strength, has dramatic effects on the stability of colloidal dispersions. At high electrolyte concentrations, the diffuse layer is compressed, and the particles approach more closely. The coarsening of the particles results in their enhanced sedimentation and subsequent phase separation. This is why the electrochemical synthesis of the composite Fe/ZrO_2 was performed under the conditions of a continuous bath agitation with a magnetic stirrer (~ 60 rev/min^{-1}). It should be noted that the reproducibility of the experimental results was quite satisfactory under the circumstances.

Electrodeposition of composite Fe/ZrO_2 coatings

As follows from the data given in Fig. 5, the content of ZrO_2 particles in the composite coatings obtained from the methanesulfonate electrolyte is appreciably higher than that in composite coatings deposited from the sulfate bath. A relatively low zirconia content in the latter case can be explained by the fact that the current efficiency of metal deposition in the sulfate electrolytes is less than 100% (in contrast to the methanesulfonate baths). Hence, the electrodeposition process is accompanied by an intensive hydrogen evolution which provides additional agitation in the near-electrode layer. Too much agitation should decrease the particle content, because the particles are ejected by a turbulent flow from the electrode surface before being incorporated [28].

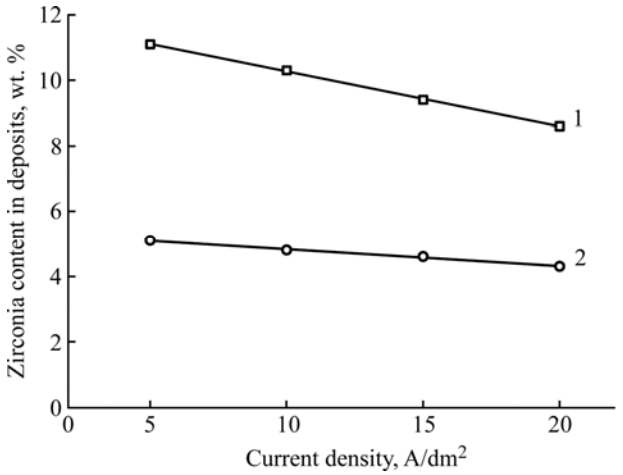

Fig. 5. Effect of current density on ZrO_2 content in composite coatings (1) in methanesulfonate electrolyte containing 1.25M $Fe(CH_3SO_3)_2$, 20 g/dm^3 ZrO_2; (2) in sulfate electrolyte containing 1.25M $FeSO_4$, 20 g/dm^3 ZrO_2. Bath temperature 298K, pH 1.3.

It is worth noting here that the composition of deposits and the current efficiency of the iron deposition do not practically depend on the electrolysis duration (Table 1).

Table 1. Content of ZrO_2 in composite coatings and current efficiency of Fe electrodeposition at different electrolysis duration

Electrolysis duration, min	ZrO_2 content, wt.%	Current efficiency, %
10	9.3	96
15	9.4	95
20	9.2	96
30	9.5	95

Bath composition: 1.25M $Fe(CH_3SO_3)_2$, 20 g/dm^3 ZrO_2; pH 1.3; temperature 298K; current density 15 A/dm^2.

The content of ZrO_2 particles in the composite coatings increases with an increase in the suspension concentration and decreases somewhat with an increase in the total current density (Fig. 6).

Many theories have been suggested in order to describe the mechanism of the composite coatings formation [19]. In this work, we applied a model proposed by Guglielmi [29]. According to this mo-

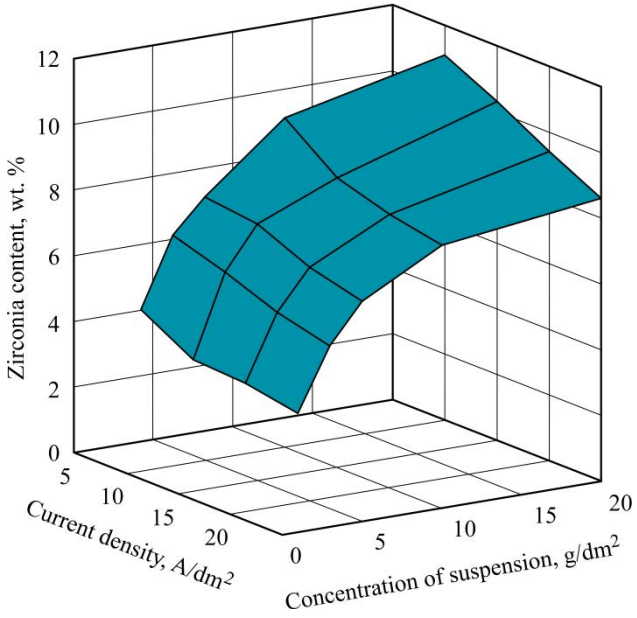

Fig. 6. Effect of current density and zirconia concentration in the bath on ZrO_2 content in composite coatings deposited from methanesulfonate electrolyte containing 1.25M $Fe(CH_3SO_3)_2$. Bath temperature 298K, pH 1.3.

del, the particles inclusion in the metallic matrix occurs in two consecutive steps of adsorption. In the first step, called a "loose adsorption", the ion-coated particles are reversibly adsorbed on the electrode surface and yield a high degree of coverage. The second step is a "strong adsorption" of particles. The reduction of metal ions adsorbed on the particles creates the circumstances of an irreversible strong adsorption. Further, the particles are engulfed by the growing of the metallic matrix. Guglielmi's model may be expressed by the following main equation

$$\frac{C}{\alpha} = \frac{Mi_0}{nF\rho_m\upsilon_0} e^{(A-B)\eta}\left(\frac{1}{k}+C\right) \qquad (4)$$

where α is the volume fraction of the particles in the coating, C is the volume fraction of the particle in the plating bath, M is the atomic weight of the electrodeposited metal, n is the valence of the deposited metal, F is the Faraday constant, ρ_m is the density of the electrodeposited metal, η is the cathodic overpotential, A is the constant in the kinetic equation of the electrochemical reaction $i = i_0 e^{A\eta}$, i_0 is the exchange current density, k is the Langmuir isotherm constant, B and υ_0 are the constants related to the particle co-deposition.

In accordance with Eq. (4), a plot of C/α vs. C at a constant current density should give a straight line, from whose intercept at $C/\alpha = 0$ the value of $(-1/k)$ can be calculated. Figure 7 presents the lines obtained for the Fe/ZrO_2 composite under study in coordinates C/α vs. C.

The intercept of all the lines at $C/\alpha = 0$ gives the value of 0.035; then the constant k is equal to 28.6 for yttria stabilized zirconia particles co-deposited with iron in methanesulfonate electrolytes.

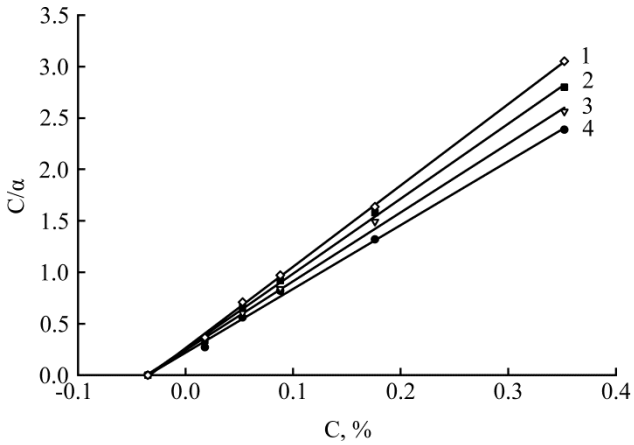

Fig. 7. Ratio C/α vs zirconia concentration in plating baths at various current densities, A/dm^2: (1) 20; (2) 15; (3) 10; (4) 5. Baths contain 1.25M $Fe(CH_3SO_3)_2$. Temperature 298K, pH 1.3.

The value of k indicates the net reaction constant of the particle adsorbed on the electrode surface and can be expressed as

$$k = \frac{k_a}{k_d} \qquad (5)$$

where k_a is the adsorption coefficient and k_d is the desorption coefficient of particles on the electrode. If $k > 1$, it indicates that the adsorption rate of particles is faster than the desorption rate [30].

Guglielmi's model implies the Langmuir adsorption isotherm modified as follows [29]:

$$\sigma = \frac{kC}{1+kC}(1-\theta) \qquad (6)$$

where σ is the loose adsorption coverage and θ is the strong adsorption coverage.

The loose adsorption coverage may be estimated by Eq. (6) if we assume that the surface coverage of the strong adsorption is close to the volume fraction of the particles ($\theta \approx \alpha$) [29].

As can be seen from the data presented in Table 2, at all current densities and ZrO_2 concentrations, the loose adsorption of the particles is much higher than their concentration in the bath. Furthermore, just a little fraction of the loosely adsorbed particles can be co-deposited by the reduction of the metallic ions surrounding them. Consequently, the rate determining step in the co-deposition of zirconia in the iron methanesulfonate plating bath is controlled by the transfer from the loose adsorption to the strong adsorption [29–31].

Table 3 gives the slopes ($tg\varphi$) of the lines which were plotted in coordinates C/α vs. C (see Fig. 7) at different current densities. For these dependences, Guglielmi deduced the following expression [29]:

$$\lg(tg\varphi) = \lg\frac{Mi_0\, B/A}{nF\rho_m\upsilon_0} + \left(1-\frac{B}{A}\right)\lg i. \qquad (7)$$

From the experimental results, the curve lg ($tg\varphi$) vs. lg i was plotted (Fig. 8). It is clear that the slope of such dependences enables the calculation

Table 2. Loose and strong adsorption coverage at various current densities and suspension concentrations

Current density, A/dm^2	ZrO_2 particles concentrations in bath, vol. %									
	0.02		0.05		0.09		0.18		0.35	
	σ %	θ %	σ %	θ %	σ %	θ %	σ %	θ %	σ %	θ %
5	31.7	6.7	54.6	9.4	63.9	10.8	72.3	13.3	77.6	14.8
10	32.1	5.5	55.0	8.8	64.1	10.5	73.6	11.8	78.5	13.7
15	32.2	5.3	55.4	8.0	64.7	9.6	74.1	11.1	79.5	12.6
20	32.3	4.9	55.8	7.5	65.1	9.1	74.5	10.8	80.5	11.5

Bath contains 1.25M $Fe(CH_3SO_3)_2$; pH 1.3; temperature 298K.

of the value *B/A*. As can be seen, the dependence lg (tgφ) vs. lg *i* consists of two linear sections with various slopes: section I (at relatively low current densities) and section II (at relatively high current densities). It should be mentioned that we have used the values of the *partial* current densities of iron deposition, calculated on the basis of the above mentioned current efficiencies (see Fig. 1), but not the *total* current densities when plotting the dependence lg (tgφ) vs. lg *i*.

Table 3. Dependence of slope of lines plotted in coordinates *C*/α vs *C* on current density

Current density, A/dm^2	tg φ
5	6.21
10	6.67
15	7.29
20	7.94

Bath contains 1.25M $Fe(CH_3SO_3)_2$; pH 1.3; temperature 298K.

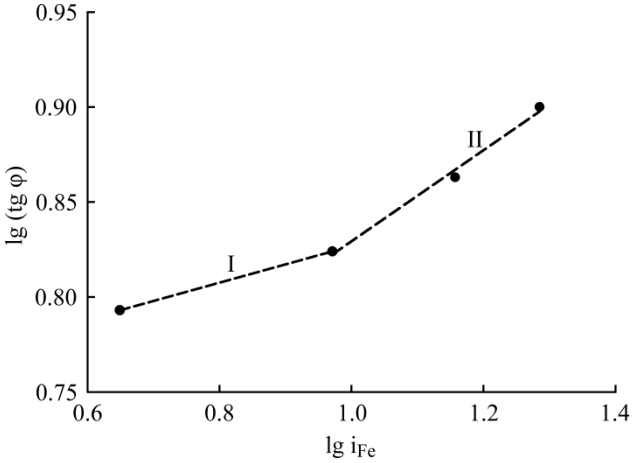

Fig. 8. Plot of lg (tgφ) versus lg *i* according to Eq. (7).

The fact that the dependence shown in Fig. 8 is not entirely linear suggests that the values *A* and (or) *B* in Eq. (4) change somewhat with the current density. It is important to underline that the value lg (tgφ) increases with an increase of lg *i* (the slopes are equal to 0.1 and 0.24 in sections I and II, respectively). Then, according to Eq. (7), the following inequality will be valid: $(1 - B/A) > 0$, i.e. $B < A$. This means that the Fe cations adsorbed on the particles are electroreduced more slowly than the solvated Fe cations [28]. In addition, the fact that *B* is lower than *A* involves a decrease of α with an increase of the current density; this conclusion is in good agreement with the experimental data obtained.

SEM investigation, EDX analysis, and XRD characterization

Figure 9 shows the typical SEM images of iron and composite iron-zirconia coatings deposited from methanesulfonate baths. The surface morphology of "pure" iron is smooth but there is a superficial network of cracks. The ZrO_2 agglomerates incorporated into the deposits structure are irregular and the surface morphology becomes heterogeneous. The ZrO_2 dispersed particles are easy to distinguish in SEM micrographs, their average size (about several μm) correlates accurately with the data of the sedimentation analysis (see above).

The EDX analysis of composite iron-zirconia coatings was performed in various areas of the surface: (i) in the region that is free from the particles entrapped, and (ii) directly in the area of the incorporated agglomerate. In agreement with these results (Table 4), the EDX analysis provided evidence that the surface of the regions without visible dispersed particles consists essentially of iron and oxygen, a small amount of zirconium being also detected.

The detection of oxygen in the region that is free from the incorporated dispersed particles can be explained by the fact that even a brief contact of the freshly deposited iron with electrolyte (after current interruption) or with atmospheric oxygen and moist air was sufficient to create a thin oxide layer on the iron surface.

The surface of the dispersed particles embedded in the coating is predictably enriched with Zr, O and Y. The EDX analysis also revealed that the surface of the dispersed particles, entrapped into the deposit, contains small amounts of such elements as sulfur, carbon, sodium and iron (together with zirconium, oxygen and yttrium). This is presumably due to the engulfment of electrolyte traces by the spongy aggregates of ZrO_2 particles. Then the source of sulfur and carbon may be MSA; iron is included as adsorbed Fe(II) ions; sodium is present in electrolyte as a result of pH adjustment by the adding of Na_2CO_3 solution.

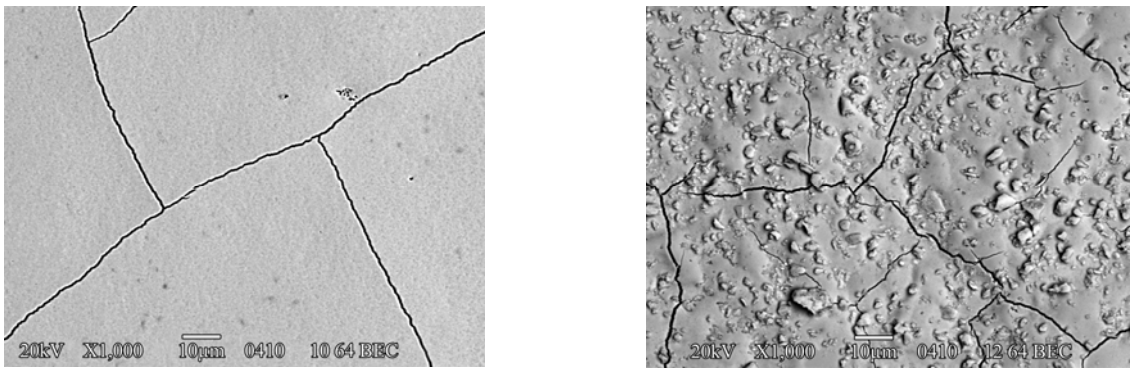

(a) (b)

Fig. 9. SEM micrographs of (a) iron and (b) iron-zirconia composite deposited at cathodic current density of 20 A/dm^2. Bath composition: (a) 1.25M $Fe(CH_3SO_3)_2$; (b) 1.25M $Fe(CH_3SO_3)_2$, 20 g/dm^3 ZrO_2. Temperature 298K, pH 1.3.

Table 4. Results of EDX analysis of the Fe/ZrO_2 composite surface

Element	Content, wt.%	
	Region free from the particles entrapped	Region of incorporated agglomerate
Fe	96.5	40.4
O	2.7	18.6
Zr	0.3	33.3
Y	–	1.7
Other elements	0.5	6.0

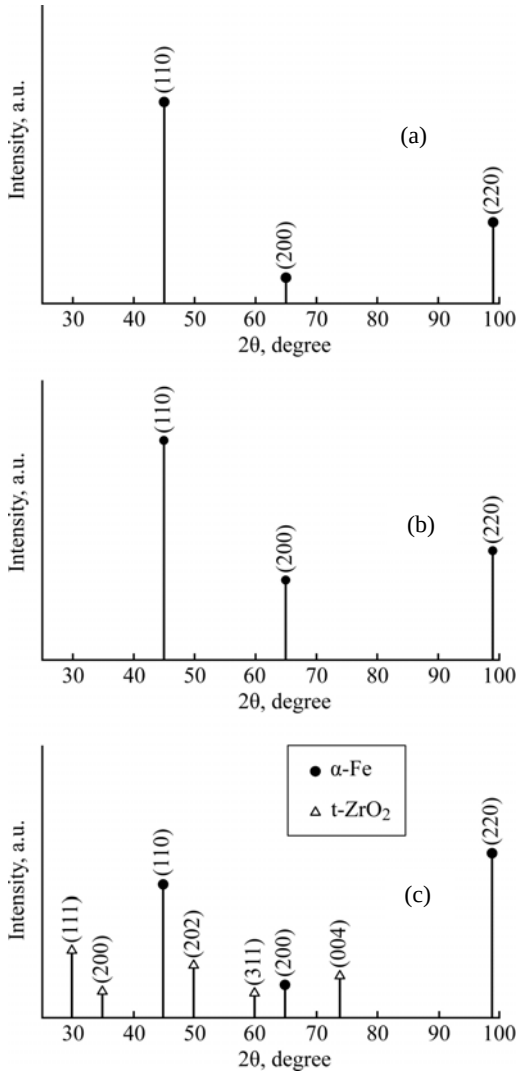

Fig. 10. XRD patterns of (a) iron coating deposited from sulfate plating bath; (b) iron coating deposited from methanesulfonate plating bath; (c) iron-zirconia composite coating deposited from methanesulfonate plating bath.

The XRD patterns of pure iron and composite iron-zirconia coatings are shown in Fig. 10. All coatings exhibit a single phase of the α-Fe matrix with the body centered cubic (bcc) lattice. ZrO_2 is present as tetragonal (*t*) phase. The reflections of the Cu foil substrate were also detectable (they are not presented in Fig. 10).

In order to estimate the Fe crystalline size, the Scherrer equation was used:

$$D = \frac{0.9\lambda}{\beta \cos\theta} \tag{8}$$

where D is the crystalline size, λ is the wavelength of X-rays, β is the corrected peak width at a half-maximum intensity and θ is the angular position.

The calculated average crystallite sizes are given in Table 5. As can be seen, the Fe coatings under study are nanocrystalline, the D value being higher for the sulfate electrolyte than that in case of a methanesulfonate bath. When iron is co-deposited with ZrO_2 particles, the crystallite size increases, although insignificantly.

Table 5. Crystallite size of Fe and Fe/ZrO_2 composite coatings

Type of coating	*D*, nm
Fe from sulfate bath	60
Fe from methanesulfonate bath	42
Fe/ZrO_2 from methanesulfonate bath	48

Microhardness of deposits

Figure 11 demonstrates the dependence of Fe electrodeposits microhardness on current density both for a sulfate bath and a methanesulfonate one. The value of microhardness increases with the current density in the range from 5 to 20 A/dm^2. At higher current densities, the microhardness remains practically unvarying. The iron coatings obtained from a methanesulfonate electrolyte are appreciably harder than those from the sulfate system. This may be caused by lowering the nano-crystallite size. Indeed, the microhardness of electrodeposits belongs to the properties which exhibit a strong grain size dependence [32]. The relationship between the microhardness and crystallite size can be expressed by the Hall-Petch equation [33, 34]:

$$H = H_0 + kd^{-1/2} \tag{9}$$

where H_0 is the microhardness value at a large grain size, d in the grain size and k is a certain constant for each material.

With reference to this equation, smaller grain sizes introduce higher grain boundary densities and, therefore, higher concentrations of obstacles for the dislocation slip. As a result, the hardness of material grows.

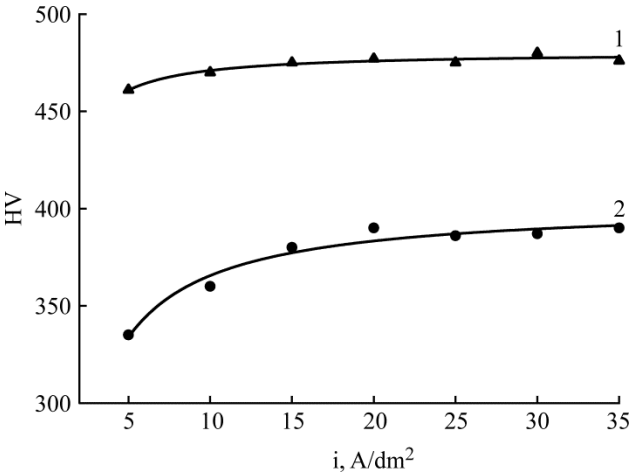

Fig. 11. Effect of current density on the microhardness of Fe deposits obtained from (1) methanesulfonate electrolyte containing 1.25M $Fe(CH_3SO_3)_2$ and (2) sulfate electrolyte containing 1.25M $FeSO_4$. Bath temperature 298K, pH 1.3.

Figure 12 shows the dependence of Vickers microhardness upon the grain size for Fe coatings in linear coordinates according to the Hall-Petch equation. For comparison, the corresponding values of nano-crystalline iron borrowed from [35] are also presented. It can be easily seen that the data obtained in this work satisfactorily coincide with the independent data given in literature.

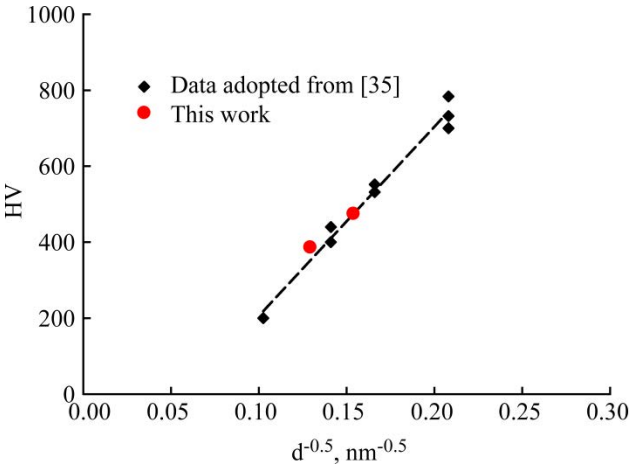

Fig. 12. Vickers microhardness versus grain size $d^{-0.5}$ for iron powder [35] and for iron nano-crystalline coatings obtained in the present work.

The introduction of yttria-stabilized ZrO_2 particles into the iron matrix leads to an appreciable increase in the microhardness of coatings (Fig. 13). A growth in the suspension concentration results in a continuous increase in the deposits microhardness.

The enhanced microhardness of composite Fe/ZrO_2 coatings in comparison with pure iron might be due to two possible hardening mechanisms, namely, the grain refinement (i.e. a strengthening effect from the Hall-Petch relationship) and the dispersion strengthening (i.e. a strengthening effect by the Orowan mechanism) [20, 36, 37]. Since embedding zirconia particles in the metal matrix does not lead to the grain refinement (see Table 5), we may

conclude that the strengthening effect from the Hall-Petch relationship is not responsible for the observed growth of the coatings hardness. A dispersion-strengthened composite is characterized by a dispersion of fine particles with an average diameter ranging from about 0.5 to 5 μm. In this case, the fine dispersed particles impede the motion of dislocations in the metallic matrix resulting in an increase in the material hardness.

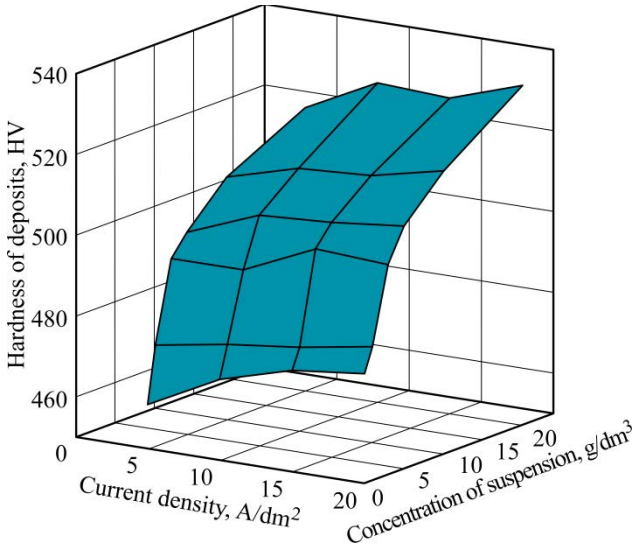

Fig. 13. Effect of current density and zirconia concentration in the bath on deposits microhardness. Electrolytes contain 1.25M $Fe(CH_3SO_3)_2$. Bath temperature 298K, pH 1.3.

To sum up, in the present study the improvement of composite coatings microhardness was achieved by the dispersion hardening effect (i.e. by the Orowan mechanism). As was reported in a number of previous publications [20, 37–39], the effect of the Orowan strengthening may be much stronger than the Hall-Petch strengthening for various composite coatings.

CONCLUSIONS

1. The CE of the iron electrodeposition reaction in a methanesulfonate electrolyte is appreciably higher than that in a typical sulfate bath. The differences in the values of the CE in the electrochemical systems under consideration are related to the features of the HER rather than to the kinetics of the metal deposition.

2. The introduction of yttria-stabilized ZrO_2 particles into the iron plating bath allows obtaining composite coatings with the zirconia content up to 10–12 wt.%. It has been shown that the aggregation of ZrO_2 nano-particles occurs in the iron plating baths and the aggregates with the average size of several micrometers are embedded in the metal matrix. The content of the zirconia phase in composite coatings increases with an increase in the suspension concentration and a decrease in the current density.

3. The mechanism of co-deposition proposed by Guglielmi proved to be valid for the Fe/ZrO_2 composite plating in a methanesulfonate electrolyte. The rate determining the step is controlled by the particles transference from the loose adsorption to the strong one.

4. Iron coatings obtained from a methanesulfonate bath are harder than those deposited from a sulfate bath due to the strengthening effect by the Hall-Petch mechanism. The inclusion of ZrO_2 particles in the iron matrix leads to the enhancement of the coatings microhardness by the dispersion strengthening mechanism.

REFERENCES

1. Díaz S.L., Calderón J.A., Barcia O.E., Mattos O.R. Electrodeposition of Iron in Sulphate Solutions. *Electrochim Acta.* 2008, **53**, 7426–7435.

2. Panayotova M. Deposition of Fe-C Alloy on Structural Steel and Cast Iron for Repair of Worn Machine Parts. *Surf Coat Technol.* 2000, **124**, 266–271.

3. Miyamoto N., Yoshida K., Matsuoka M., Tamaki J. Effect of Phosphorus Content on Mechanical Properties of Electrodeposited Fe-C-P Alloys. *J Electrochem Soc.* 2004, **151**, C645–C648.

4. Lallemand F., Ricq L., Wery M., Berçot P., Pagetti J. The Influence of Organic Additives on the Electrodeposition of Iron-group Metals and Binary Alloy from Sulfate Electrolyte. *Appl Surf Sci.* 2004, **228**, 326–333.

5. Danilov F.I., Protsenko V.S., Ubiikon' A.V. Kinetic Regularities Governing the Reaction of Electrodeposition of Iron from Solutions of Citrate Complexes of Iron (III). *Russ J Electrochem.* 2005, **41**, 1282–1289.

6. Pan B., Fang X., Tian Y. Electrodeposition of Fe-diamond Composite Material for Manufacture of Diamond Tools. *Appl Mech Mater.* 2010, **37-38**, 398–401.

7. Zhou P., Zhong Y., Wang H., Fan L., Dong L., Li F., Long Q., Zheng T. Behavior of Fe/nano-Si Particles Composite Electrodeposition with a Vertical Electrode System in a Static Parallel Magnetic Field. *Electrochim Acta.* 2013, **111**, 126–135.

8. Gernon M.D., Wu M., Buszta T., Janney P. Environmental Benefits of Methanesulfonic Acid: Comparative Properties and Advantages. *Green Chem.* 1999, **1**, 127–140.

9. Finšgar M., Milošev I. Corrosion Behaviour of Stainless Steels in Aqueous Solutions of Methanesulfonic Acid. *Corros Sci.* 2010, **52**, 2430–2438.

10. Balaji R., Pushpavanam M. Methanesulphonic Acid in Electroplating Related Metal Finishing Industries. *Trans Inst Met Finish.* 2003, **81**(5), 154–158.

11. Martyak N.M., Seefeldt R. Additive-effects During Plating in Acid Tin Methanesulfonate Electrolytes. *Electrochim Acta.* 2004, **49**, 4303–4311.

12. Protsenko V.S., Kityk A.A., Danilov F.I. Kinetics and Mechanism of Chromium Electrodeposition from Methanesulfonate Solutions of Cr(III) Salts. *Surf Eng Appl Electrochem.* 2014, **50**(5), 384–389.

13. Low C.T.J., Walsh F.C. Electrodeposition of Tin, Copper and Tin-copper Alloys from a Methanesulfonic Acid Electrolyte Containing a Perfluorinated Cationic Surfactant. *Surf Coat Technol.* 2008, **202**, 1339–1349.

14. Danilov F.I., Protsenko V.S., Vasil'eva E.A., Kabat O.S. Antifriction Coatings of Pb-Sn-Cu Alloy Electrodeposited from Methanesulphonate Bath. *Trans Inst*

Metal Finish. 2011, **89**(3), 151–154.

15. Mohan S., Vijayakumar J., Saravanan G. Influence of CH_3SO_3H and $AlCl_3$ in Direct and Pulse Current Electrodeposition of Trivalent Chromium. *Surf Eng.* 2009, **25**, 570–576.
16. Sidel'nikova S.P., Petrov Yu.N., Gorodetskii Yu.S. Investigation of the Cathodic Polarization and Hydrogenation of Deposits in the Electrodeposition of Iron from Methylsulfate and Sulfate Electrolytes. *Prot. Met.* 1974, **10**, 177–179.
17. Pleshka E.D. Adhesion of Iron Coatings with Steel and Cast Iron. *Surf Eng Appl Electrochem*. 2008, **44**(2), 92–97.
18. Pleshka E.D. Iron Coatings from Multicomponent Methyl Sulfate Chloride Electrolyte. *Surf Eng Appl Electrochem*. 2008, **44**(4), 264–270.
19. Low C.T.J., Wills R.G.A., Walsh F.C. Electrodeposition of Composite Coatings Containing Nanoparticles in a Metal Deposit. *Surf Coat Technol.* 2006, **201**, 371–383.
20. Wang W., Hou F.-Y., Wang H., Guo H.-T. Fabrication and Characterization of Ni-ZrO_2 Composite Nano-coatings by Pulse Electrodeposition. *Scripta Mater*. 2005, **53**, 613–618.
21. Huang J.M., Li Y., Zhang G.F., Hou X.D., Deng D.W. Electroplating of Ni-ZrO_2 Nanocomposite Coatings on 40CrNiMo7 Alloy. *Surf Eng.* 2013, **29**, 194–199.
22. Hou F., Wang W., Guo H. Effect of the Dispersibility of ZrO_2 Nanoparticles in Ni-ZrO_2 Electroplated Nanocomposite Coatings on the Mechanical Properties of Nanocomposite Coatings. *Appl Surf Sci.* 2006, **252**, 3812–3817.
23. Vasil'eva E.A., Smenova I.V., Protsenko V.S., Konstantinova T.E., Danilov F.I. Electrodeposition of Hard Iron–zirconia Dioxide Composite Coatings from a Methanesulfonate Electrolyte. *Russ J Appl Chem.* 2013, **86**, 1735–1740.
24. Slipenyuk A.M., Glinchuk M.D., Bykov I.P., Ragulya A.V., Klimenko V.P., Konstantinova T.E., Danilenko I.A. ESR Investigation of Yttria Stabilized Zirconia Powders with Nanosize Particles. *Ferroelectrics* 2004, **298**, 289–296.
25. Konstantinova T.E., Ragulya A.V., Doroshkevich A.S., Volkova G.K., Glazunova V.A. The Mechanism of Particle Formation in Y-doped ZrO_2. *Int J Nanotechnol*. 2006, **3**, 29–38.
26. Yashchishyn I.A., Korduban A.M., Konstantinova T.E., Danilenko I.A., Volkova G.K., Glazunova V.A., Kandyba V.O. Structure and Surface Characterization of ZrO_2–Y_2O_3–Cr_2O_3 System. *Appl Surf Sci.* 2010, **256**, 7175–7177.
27. Zech N., Landolt D. The Influence of Boric Acid and Sulfate Ions on the Hydrogen Formation in Ni-Fe Plating Electrolytes. *Electrochim Acta.* 2000, **45**, 3461–3471.
28. Berçot P., Peña-Muñoz E., Pagetti J. Electrolytic Composite Ni-PTFE Coatings: an Adaptation of Guglielmi's Model for the Phenomena of Incorporation. *Surf Coat Technol.* 2002, **157**, 282–289.
29. Guglielmi N. Kinetics of the Deposition of Inert Particles from Electrolytic Baths. *J Electrochem Soc.* 1972, **119**, 1009–1012.
30. Wang S.-C., Wei W.-C. J. Kinetics of Electroplating Process of Nano-sized Ceramic Particle/Ni Composite. *Mater Chem Phys.* 2003, **78**, 574–580.
31. Bahadormanesh B., Dolati A. The Kinetics of Ni–Co/SiC Composite Coatings Electrodeposition. *J Alloys Compd.* 2010, **504**, 514–518.
32. Erb U. Size Effects in Electroformed Nanomaterials. *Key Eng Mater.* 2010, **444**, 163–188.
33. Hall E.O. The Deformation and Ageing of Mild Steel: III Discussion of Results. *Proc Phys Soc. B* 1951, **64**, 747–753.
34. Petch N.J. The Upper Yield Stress of Polycrystalline Iron. *Acta Metall.* 1964, **12**, 59–65.
35. Khan A.S., Zhang H., Takacs L. Mechanical Response and Modeling of Fully Compacted Nanocrystalline Iron and Copper. *Int J Plast.* 2000, **16**, 1459–1476.
36. Mohajeri S., Dolati A. Electrodeposition of Ni/WC Nano composite in Sulfate Solution. *Mater Chem Phys.* 2011, **129**, 746–750.
37. Aghaie E., Najafi A., Maleki-Ghaleh H., Mohebi H. Effect of SiC Concentration in Electrolyte on Ni-SiC Composite Coating Properties. *Surf Eng.* 2013, **29**, 177–182.
38. Gyftou P., Pavlatou E.A., Spyrellis N. Effect of Pulse Electrodeposition Parameters on the Properties of Ni/nano-SiC Composites. *Appl Surf Sci.* 2008, **254**, 5910–5916.
39. Mokabber T., Rastegari S., Razavizadeh H. Effect of Electroplating Parameters on Properties of Zn-nano-TiO_2 Composite Coatings. *Surf Eng.* 2013, **29**, 41–45.

Received 22.04.14
Accepted 05.05.14

Реферат

Исследовано электроосаждение железных и композиционных железо-диоксидно-циркониевых покрытий из метансульфонатного электролита. Установлено, что выход по току реакции осаждения железа в метансульфонатном электролите существенно выше, чем в обычном сульфатном электролите. Железные покрытия, электроосажденные из метансульфонатного электролита, обладают нанокристаллической структурой. Fe осадки, полученные из метансульфонатных электролитов, отличаются большей твердостью в сравнении с покрытиями, осажденными из сульфатных электролитов, в результате проявления эффекта упрочнения по механизму Хэлла-Петча. Композиционные Fe/ZrO_2 покрытия могут быть получены из электролитов железнения, содержащих частицы диоксида циркония, стабилизированного 3 мол. % оксида иттрия. Кинетика соосаждения частиц ZrO_2 с железом из метансульфонатных электролитов описывается моделью Гуглиельми. Включение частиц диоксида циркония в железную матрицу приводит к существенному увеличению микротвердости вследствие механизма дисперсионного упрочнения.

Ключевые слова: электроосаждение, железо, диоксид циркония, композиционное покрытие, метансульфонатный электролит.